# Change in aneurysmal flow pulsatility after flow diverter treatment

Ignacio Larrabide[a,*], Arjan J. Geers[b], Hernán G. Morales[c], Daniel, A. Rüfenacht[d]

[a] *PLADEMA-CONICET, Universidad Nacional del Centro de la Provincia de Buenos Aires, Tandil, Argentina*
[b] *Universitat Pompeu Fabra, Barcelona, Spain*
[c] *Medisys, Philips Research Paris, France*
[d] *Hirslanden Clinic, Zürich, Switzerland*

**Abstract**

**Motivation:** Treatment of intracranial aneurysms with flow diverters (FDs) has recently become an attractive alternative. Although considerable effort has been devoted to understand their effects on the time-averaged or peak systolic flow field, no previous study has analyzed the variability of FD-induced flow reduction along the cardiac cycle.

**Methods:** Fourteen saccular aneurysms, candidates for FD treatment because of their morphology, located on the internal carotid artery were virtually treated with FDs and pre- and post-treatment blood flow was simulated with CFD techniques. Common hemodynamic variables were recorded at each time step of the cardiac cycle and differences between the untreated and treated models were assessed.

**Results:** Flow pulsatility, expressed by the pulsatility index (PI) of the velocity, significantly increased (36.0 %; range: 14.6 % to 88.3 %) after FD treatment. Peak systole velocity reduction was significantly smaller (30.5 %; range: 19.6 % to 51.0 %) than time-averaged velocity reduction (43.0 %; range: 29.1 % to 69.8 %). No changes were observed in the aneurysmal pressure.

**Conclusions:** FD-induced flow reduction varies considerably during the

*Corresponding author
*Email address:* ignacio.larrabide@gmail.com (Ignacio Larrabide)

cardiac cycle. FD treatment significantly increased the flow pulsatility in the aneurysm.

*Keywords:* Intracranial aneurysms, flow diverter, velocity, WSS, time dependency

---

## 1. INTRODUCTION

Flow diverters (FDs) have in recent years become an attractive alternative to treat cerebral aneurysms [1, 2]. These endovascular devices are low-porosity stents, placed in the parent artery to divert blood flow away from the aneurysm. The flow reduction is aimed at promoting thrombosis inside the aneurysm and effectively excluding it from blood circulation. In particular, wide-necked, fusiform and giant aneurysms are well-suited for this treatment option [3].

Hemodynamic changes after FD treatment have been extensively studied using computational fluid dynamics (CFD), both for idealized [4, 5, 6] and anatomically realistic vascular geometries [7, 8, 9, 10, 11, 12, 13, 14]. Many studies have focused on quantifying flow reduction as a measure of treatment performance and evaluating its dependency on stent design and configuration [4, 5, 8], aneurysm morphology [5, 10, 6] and inflow rate boundary conditions [14]. Others have replicated specific treatments to investigate associations between treatment outcome and hemodynamics [7, 9, 11, 12, 13]. Primarily, the performance of FDs has been evaluated by considering the time-averaged or peak systolic flow field, but as the performance may vary during the cardiac cycle [15], analyzing changes in the aneurysmal flow dynamics could provide relevant additional information.

Although animal experiments, CFD studies and clinical series have already shown impressive effectiveness of this technology, the effects on local hemodynamics are yet not fully understood [16, 17, 7]. Besides complete aneurysm occlusions in the majority of the cases, longer term persisting patency and delayed aneurysm ruptures have also been reported after FD treatment. Since the advent of the technology, different studies have been developed to model these devices and to provide a better understanding of their effect on hemodynamics. The aim of this study was to determine the effect of FDs on the flow pulsatility inside the aneurysm during the cardiac cycle, by considering that the hydraulic resistance of the flow diverter depends on the Reynolds number.


Figure 1: Surface models for the 14 cases analyzed in this study.

## 2. MATERIALS AND METHODS

### *2.1. Materials*

Fourteen vascular models of the internal carotid artery (ICA) harbouring saccular aneurysms were included in this study (Fig. 1). All images were acquired at the Hôpitaux Universitaires de Geneva, Switzerland, and processed following a data processing protocol previously described [18]. All aneurysm were located at the internal carotid artery to reduce the hemodynamic variability due to different vascular morphology [19]. Anatomical models, represented by triangular surface meshes, were constructed by segmenting three-dimensional rotational angiography (3DRA) images using a geodesic active regions approach [20] and manually performing mesh cleaning, hole filling and smoothing operations [21]. Images were acquired with an Integris$^{TM}$ Allura System (Philips Healthcare, Best, The Netherlands). Voxel sizes in the reconstructed 3D images were $0.208 \times 0.208 \times 0.208$ mm.

The 14 cases used in ths study where selected by three clinicians as being most appropriate for endovascular FD treatment. Their criteria for selecting the treatment was 1) the aneurysm was suboptimal for treatment with coils because of its morphology and/or neck width and 2) the absence of branching arteries (typically ophtalmic artery or the anterior choroidal artery) nearby the aneurysm that could be occluded by the device.

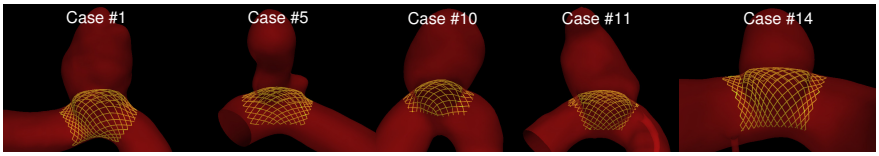


Figure 2: Vascular models with deployed FDs. Only the portion of the FD covering the aneurysm neck was kept for the CFD simulation. Some vessels were truncated to prevent them from blocking the view. The complete vasculatures are shown in Fig. 1.

### *2.2. Flow diverter models*

The Fast Virtual Stenting (FVS) method was used [22] for the virtual placement of FDs in the vascular models. The stent struts and their connectivity were defined over a subset of points of a 2-simplex mesh with a size of $4 \times 4$, which was repeated 24 times circumferentially (resulting in 48 wires, 24 rotating right and 24 rotating left). The number of longitudinal repetitions varied between models depending on the used FD length, ensuring full coverage of the aneurysm neck and one extra diameter on each side of the aneurysm. For more details on the FVS method we refer the reader to [22]. The diameter of the stent wires was 60 microns. Portions of the stent laying on the vessel wall were removed to reduce computational time, following previous studies [23]. The FD models used were generic and did not mimic the device of any particular manufacturer intentionally, as there is variability between their designs (wire thickness, brading angulation, etc.) and the aim of this study is to remain generic. The mean±SD porosity of the FD across the neck among all cases was 75.20±2.66, ranging from 70.40% and 80.85%. In Fig. 2 are presented the resulting FD geometries used for the CFD models for 6 selected cases.

### *2.3. Computational Fluid Dynamics analysis*

Volumetric meshes were generated using ICEM CFD software package, Version 11.0 (ANSYS, Canonsburg, Pennsylvania). Meshes were composed of unstructured tetrahedral in the lumen and 6-node prism elements near the vessel wall. Smaller tetrahedral elements were used to resolve the stent struts. To ensure CFD simulations independent from mesh element size, in particular around

the FDs, a mesh independency analysis was carried out. The convergence criterion of mesh independence was that wall shear stress (WSS) and intra-aneurysmal velocity had to be within 2.5 % from the finest tested mesh. Convergence was reached with an element size around the stent strut of 0.016 mm, 3 prism layers with a total size of 0.3 mm defined everywhere but in the region of the FDs and a global tetrahedral element size of 0.3 mm. The total number of mesh elements ranged from 0.4 to 3.4 million elements for the untreated cases and from 2.6 to 15.2 million elements for the treated ones.

Unsteady CFD simulations for both treated and untreated geometrical models were performed with CFX, Version 11.0 (ANSYS), which uses a finite volume approach to solve the Navier-Stokes equations. Blood was modeled as an incompressible Newtonian fluid (density density = 1066 $\mathrm{kg/m^3}$ and viscosity = 0.0035 Pa s. A Newtonian fluid was used since viscosity changes can be neglected inside the aneurysm and artery [24]. The vessel wall was assumed to be rigid with a no-slip boundary condition. A flow rate waveform was imposed at the inlet and pressure waveforms at the outlets, all derived from a 1D mathematical model of the systemic arterial tree. A straight extension was added to the vascular model inlet and a flat velocity profile was imposed at the inlet of the extension. The combination of the extension and the considered vascular region causes the effects of the imposed velocity profile to vanish at the location of the aneurysm. The shape and average flow rate of the flow rate waveforms were the same ensuring equivalent conditions in all cases. Cardiac cycles of 0.8 s were discretized in time steps of 0.005 s. Previous studies showed that this is sufficient to provide time discretization independent solutions [25]. To remove the effect of initial transients, three complete cardiac cycles were computed and data from the last one was stored and analyzed.

### *2.4. Data analysis*

Four hemodynamic variables were analyzed, namely: 1. spatial average of intra-aneurysmal velocity magnitude ($velsa$), 2. spatial average of wall shear stress on the aneurysm wall ($wsssa$), 3. spatial average of intra-aneurysmal pres-

sure (*pressuresa*), and 4. range of intra-aneurysmal pressure (*pressurerng*), which was defined as the difference between the maximum and minimum intra-aneurysmal pressure. Variable values were recorded at each time step of the cardiac cycle. These variables were chosen for their role in aneurysm occlusion and their relation to aneurysm flow velocity [26, 27, 7, 10].

For part of the analysis, we highlighted changes in the shape and amplitude of the variables' time curves, and removed information about the absolute reduction, by normalizing variable $x$ by its time-averaged, or mean, value:

$$x_{\text{normalized}} = x/mean(x). \tag{1}$$

To assess changes in the aneurysmal flow dynamics, the pulsatility index (PI) was computed for *velsa* using Equation (2). PI measures the amplitude of *velsa* along the cardiac cycle with respect to the mean *velsa*. In other words, if PI $> 1$, the amplitude of *velsa* is larger than the mean value, and viceversa. PI is a simple measure to characterize the transient behaviour of *velsa* and is defined as:

$$\text{PI} = (max(velsa) - min(velsa))/mean(velsa). \tag{2}$$

FD-induced reductions in variable $x$ were expressed relative to the untreated condition:

$$x_{\text{reduction}} = (x_{\text{untreated}} - x_{\text{treated}})/x_{\text{untreated}}. \tag{3}$$

The Wilcoxon signed rank test was used to test the significance of differences between the untreated and treated models. Differences were considered statistically significant for $p < 0.001$.

## 3. RESULTS

Figure 3 shows *velsa* time curves together with velocity contour plots on a plane across the aneurysm before and after treatment. The plane was chosen to best visualize the main flow jet. The color map range was normalized by the space-averaged velocity inside the aneurysm at each time instant to highlight the velocity distribution rather than the magnitude. Contour plots were selected

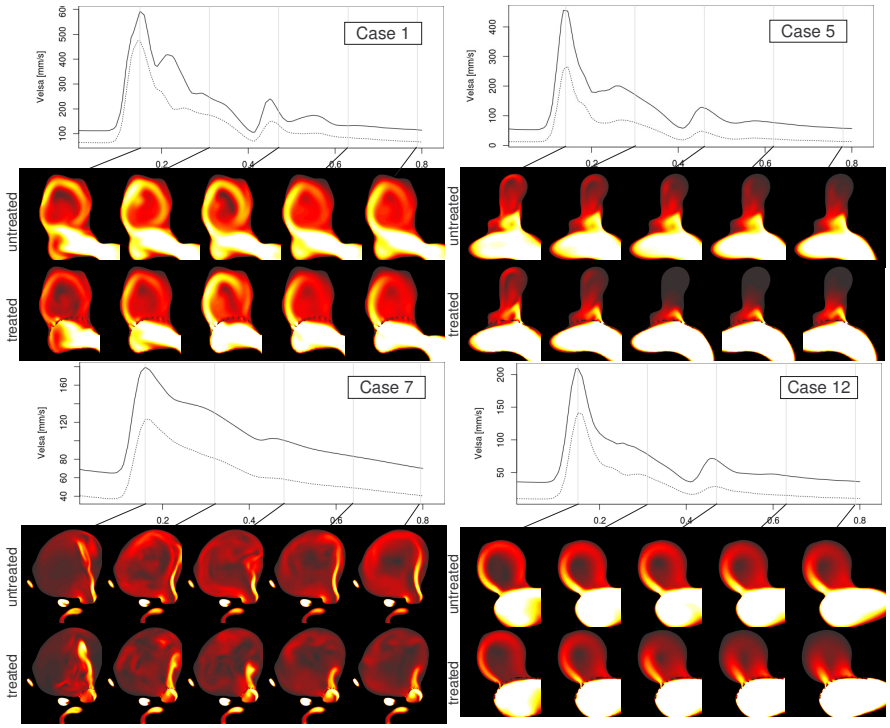


Figure 3: Time curves of *velsa* and contour plots on a cut plane through the aneurysm for different instants in the cardiac cycle before and after treatment.

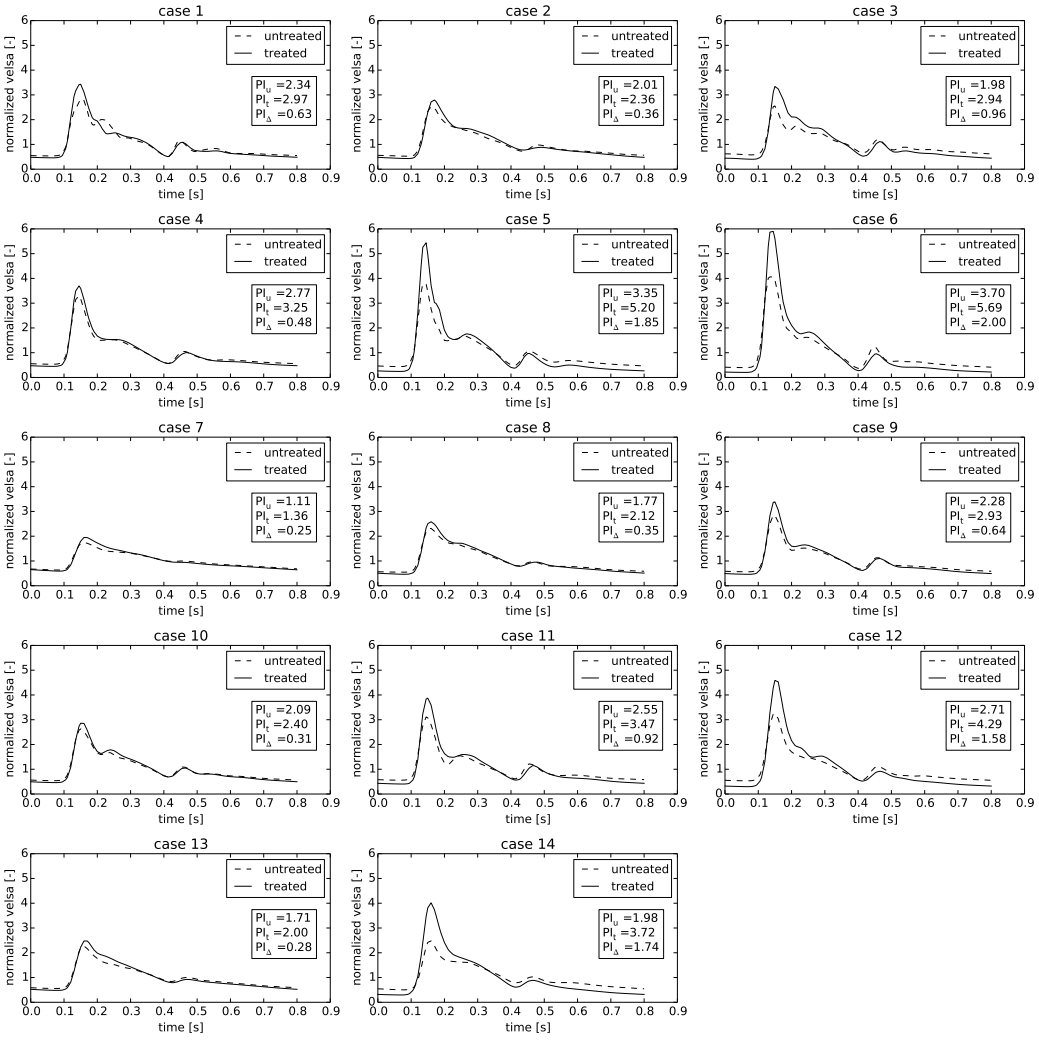


Figure 4: Normalized *velsa* curves for all cases. PI of the untreated ($PI_u$) and treated ($PI_t$) models, as well as the difference between them ($PI_\Delta$), are presented.

at peak systole and 4 other equally spaced time instants. Animations of these contour plots, for all 14 cases, are provided as supplementary material. After treatment, flow was diverted away from the aneurysm and *velsa* was visibly reduced at each time instant of the cardiac cycle. However, the main flow jet entering the aneurysm mostly preserved its direction.

Figure 4 shows for each case the normalized *velsa* along the cardiac cycle. PIs before and after FD placement, and their difference, are indicated. Although the time-averaged *velsa* was considerably decreased after FD placement, there was an increase in the amplitude of the normalized *velsa*. This result was also reflected by a significant increase in PI (mean over all 14 cases: 36.0 %; range: 14.6 % to 88.3 %). In other words, the impact of the FDs on the intra-aneurysmal flow field depends on the phase of the cardiac cycle. To better visualize this dependency, Figure 6 shows the difference between the normalized *velsa* plots ('untreated - treated'), as well as the differences between normalized plots of *wsssa*, *pressuresa* and *pressurerng*. The difference is positive for above average reduction and negative for below average reduction. In the figure, the left column shows the absolute difference of the normalized curves for all cases and the right column shows the average curve. In general, the relative reductions of *velsa*, *wsssa* and *pressurerng* were larger (above mean reduction) during late diastole and smaller during peak systole. With respect to the other variables, the changes in *pressuresa* were insignificant. This indicates that FD placement did not induce significant increases or decreases in intra-aneurysmal pressure.

Figure 5 shows boxplots to compare reductions between the peak systolic and time-averaged flow fields. The reduction of *velsa* during peak systole was significantly lower (mean: 30.5 %; range: 19.6 % to 51.0 %) than the reduction of time-averaged *velsa* (mean: 43.0 %; range: 29.1 % to 69.8 %). Similar significant differences in reduction were found for *wsssa* (time-averaged: 52.3 %; peak systolic: 40.5 %) and *pressurerng* (time-averaged: 55.2 %; peak systolic: 40.4 %). The *pressuresa* showed only a very slight change, both increase and decrease, after FD treatment, with no significant differences along the cardiac cycle (time-averaged: 0.1 %; peak systolic: 0.1 %).

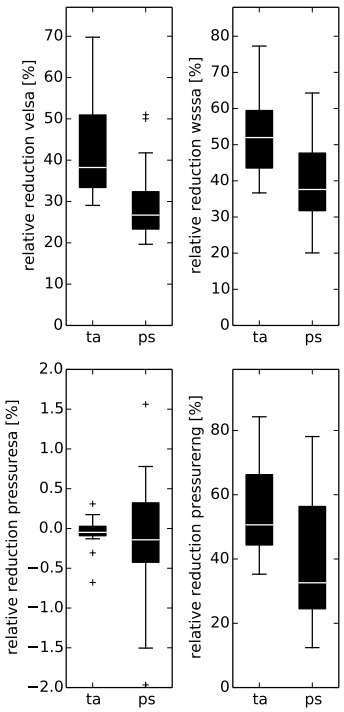


Figure 5: Boxplots showing the relative reduction for *velsa*, *wsssa*, *pressuresa* and *pressurerng*. The reduction of the time-averaged (ta) value was significantly higher than the reduction of the peak systolic (ps) value for *velsa*, *wsssa* and *pressurerng*.

By its definition, PI is independent of the signal magnitude. Therefore, in the situation that flow after FD placement would be very small (e.g., 10% or less), the PI would still be large even if the flow would be negligible. To assess this, we have measured time averaged inflow into the aneurysm after FD placement and this was 63%10% (meanSTD) compared to that before treatment. The same study was performed for the time averaged velocity in the aneurysm with similar outcome (57%13%).

## 4. DISCUSSION

The aim of this study was to determine the effect of FDs on the flow pulsatility inside the aneurysm. Since the hydraulic resistance exerted by the FD mesh depends on the velocity of the flowing blood, we expected the relative reduction

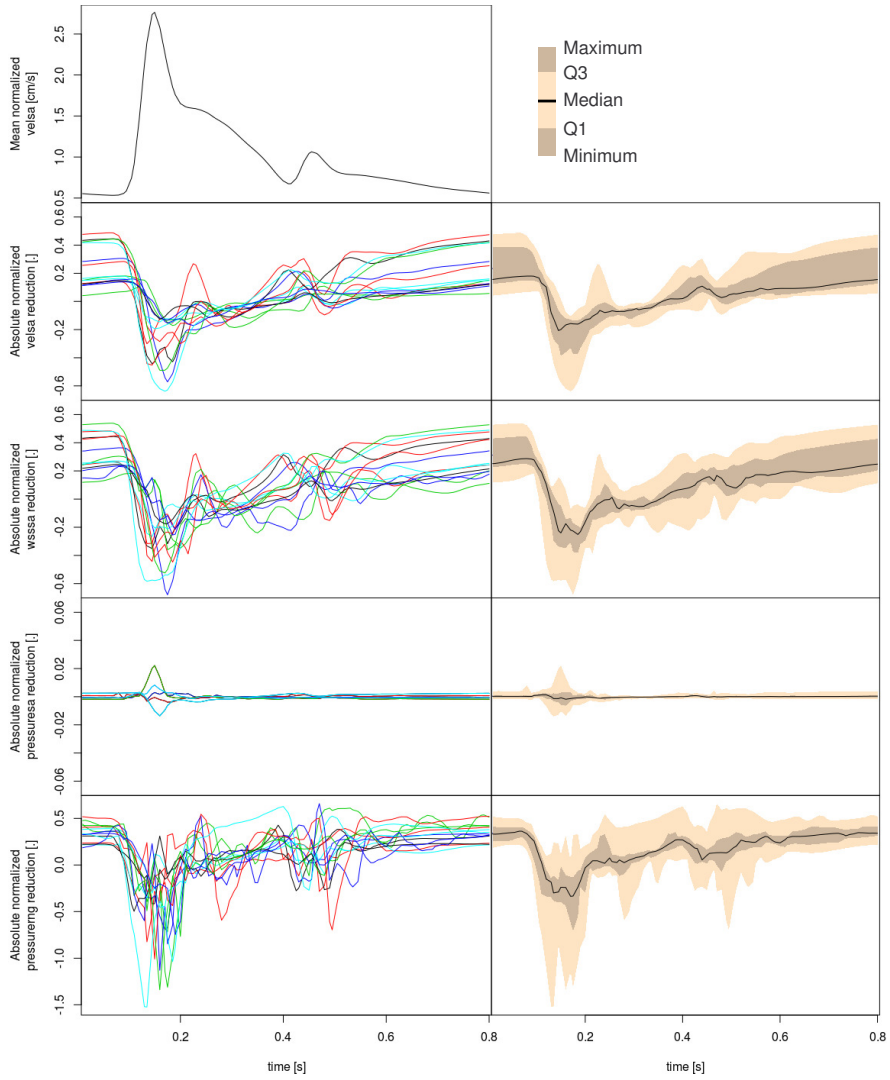


Figure 6: Difference ("untreated - treated") between the normalized *velsa*, *wsssa*, *pressuresa* and *pressurerng* plots along the cardiac cycle. The left column shows the difference curve for all cases and the right column shows their average. Q1 and Q3 represent the first and third quartile, respectively. Note that the plot range for *pressuresa* is one order of magnitude smaller than for other variables.

of the intra-aneurysmal velocity to vary during the cardiac cyle.

The hydraulic resistance to flow across the FD mesh is due to the blockage that the FD exerts on the flow entering the aneurysm. This resistance depends on the Reynolds number [28, 29] and combines frictional and pressure drags. Kim et at. performed a detailed experimentation of the hydraulic resistance for high porosity stents on an idealized aneurysm model. They found that stent porosity is an important factor influencing the resistance to flow. Hydraulic resistance increases with decreasing porosity. Most importantly, they confirmed that the resistance to flow, for a given stent, is reduced when increasing the Reynolds number [29].

Because arterial flow is pulsatile, the flow velocity changes along the cardiac cycle. Therefore, from the reasoning above, the flow reduction exerted by a FD, i.e. its performance, could be expected to change during the cardiac cycle. This hypothesis was evaluated and confirmed in our study. During systole, the flow velocity was considerably higher (twice or more) than during diastole. As a result, the pressure gradient across the FD mesh during systole was smaller than during diastole, which resulted in larger relative reductions when the velocity was effectively slower. This also explains the fact that in fusiform aneurysms, where it is usual to find that the main inflow jet and the highest velocities go straight into the aneurysm and across the FD mesh, the reductions are lower than in saccular ones [10].

After FD placement, an increase of PI occurred in every case. This was explained by the relative increase in the *velsa* curve amplitude. We could observe that, although the mean velocity was reduced along the cardiac cycle, the velocity peaks occurring in systole were far from being completely smoothed out. In fact, the difference relative to the mean *velsa* between systolic and diastolic intra-aneurysmal velocity increased, leading to higher PIs. As observed in Figure 4, in every case the maximum value of the normalized *velsa* was increased and the minimum was decreased. The effect of the FD was to slow down intra-aneurysmal velocity, but the FD was not capable of flattening down the flow velocity differences along the cardiac cycle and making one homogeneous flow

rate into the aneurysm along time. From this, we can say that the reduction in peak systole is the lower limit for the flow velocity reduction along the whole cardiac cycle, which is a contribution of this work. We highlight that the change after treatment will imply a change in PI, which is irrespective of the magnitude of the flow velocity, but still aneurysm inflow and flow velocity in the aneurysm remain significant.

Because depending on the aneurysm and vessel anatomy the inflow jet and its distribution can be drastically different between cases, a proper analysis of flow magnitude and its distribution should be performed when assessing the effectiveness of treatment using CFD. For instance, if regions of very low velocity exist inside the aneurysm that are washed out during systole and after the treatment, we would expect that chances of aneurysm thrombosis are relatively low. On the other hand, if the velocity is kept lower along the whole cardiac cycle, the chances of thrombus formation by stagnation are higher. As it has been proven in the literature, in many cases the aneurysm occlusion by thrombosis is progressive, and the slow growth and persistence of the thrombus is crucial [9]. No biological or clinical data reflecting the actual thrombosis of the studied cases was obtained in the present study, which should be considered in future studies [30].

During systole, *velsa* drastically increased, reaching up to a four fold when compared to late diastolic flow. Because of the changes in flow into the aneurysm in such a short period of time right after systole, it is expected unstable flow in the parent vessel and into the aneurysm. Still, as observed from Figure 3, the flow across the aneurysm neck was typically characterized by a high velocity jet and low velocity regions. After the placement of the FD, and although the jet is clearly damped, the shape and distribution of the velocity magnitude contour maps remained almost constant. When we concentrate on the different instants in time, we observe that during diastole the FD is much more effective in redirecting the flow, and the high velocities are mostly observed at the location of the parent vessel, while the inflow jet is strongly diffused. These differences in flow reduction during systole and diastole might be relevant for the design of

FDs in the future.

The variation in pressure due to the placement of FD was also analyzed, but no variations in *pressuresa* were observed. As outlined in previous publications, the flow diverters are not pressure diverters [7, 31, 10]. A FD produces minimal changes in the pressure magnitude inside the aneurysm. Still, this does not imply that the pressure distribution is not altered after FD placement. Figure 6 shows the *pressurerng* changes, comparing the pre- and post-treatment conditions. We observed that *pressurerng* was strongly altered during the cardiac cycle. This variable quantifies the difference between the maximum and the minimum pressure.

The models used in this study consider rigid walls for the vessel and the aneurysm. Also, the FD is considered to be rigid and not affected or altered by the passing flow. This a modeling choice, because the aneurysm and the vessel wall are compliant to the changes in hydrostatic pressure. Therefore, this hypothesis assumes that only minor changes would occur, which would not change the observations presented in this study. The use of Fluid Structure Interaction (FSI) CFD models would account for such changes, but difficulties arising from material properties of the aneurysm and vessel wall that are currently not possible to assess would need to be accounted for.

## 5. CONCLUSIONS

The performance of FDs strongly varies during the cardiac cycle, with lower relative flow reductions at peak systole than on average. As a result, FD treatment significantly increases the flow pulsatility in an aneurysm. Although flow is reduced throughout the cardiac cycle, flow rate changes during the cardiac cycle should be taken into account and the reduction at peak systole should be considered as lower limit.

## ACKNOWLEDGMENTS

This research has been partially funded by the Catalonian Department of Innovation, Universities and Enterprise (DIUE), through the EndoTreat project

(exp. VALOR2010-00064).

## REFERENCES

[1] P. Lylyk, C. Miranda, R. Ceratto, A. Ferrario, E. Scrivano, H. R. Luna, A. L. Berez, Q. Tran, P. K. Nelson, D. Fiorella, Curative endovascular reconstruction of cerebral aneurysms with the pipeline embolization device: The Buenos Aires experience, Neurosurgery 64 (4) (2009) 632–642.

[2] I. Szikora, Z. Berentei, Z. Kulcsar, M. Marosfoi, Z. S. Vajda, W. Lee, A. Berez, P. K. Nelson, Treatment of intracranial aneurysms by functional reconstruction of the parent artery: The Budapest experience with the pipeline embolization device, American Journal of Neuroradiology 31 (6) (2010) 1139–1147.

[3] P. K. Nelson, P. Lylyk, I. Szikora, S. G. Wetzel, I. Wanke, D. Fiorella, The pipeline embolization device for the intracranial treatment of aneurysms trial, American Journal of Neuroradiology 32 (1) (2011) 34–40.

[4] T. M. Liou, Y. C. Li, Effects of stent porosity on hemodynamics in a sidewall aneurysm model, Journal of Biomechanics 41 (6) (2008) 1174–1183.

[5] S. Seshadhri, G. Janiga, O. Beuing, M. Skalej, D. Thevenin, Impact of stents and flow diverters on hemodynamics in idealized aneurysm models, Journal of Biomechanical Engineering 133 (7) (2011) 071005.

[6] Y. F. Wu, P. F. Yang, J. Shen, Q. H. Huang, X. Zhang, Y. Qian, J. M. Liu, A comparison of the hemodynamic effects of flow diverters on wide-necked and narrow-necked cerebral aneurysms, Journal of Clinical Neuroscience: Official Journal of the Neurosurgical Society of Australasia 19 (11) (2012) 1520–1524.

[7] J. R. Cebral, F. Mut, M. Raschi, E. Scrivano, R. Ceratto, P. Lylyk, C. M. Putman, Aneurysm rupture following treatment with flow-diverting stents:

Computational hemodynamics analysis of treatment, American Journal of Neuroradiology 32 (1) (2011) 27–33.

[8] M. Tremmel, J. Xiang, S. K. Natarajan, L. N. Hopkins, A. H. Siddiqui, E. I. Levy, H. Meng, Alteration of intra-aneurysmal hemodynamics for flow diversion using enterprise and vision stents, World Neurosurgery 74 (2–3) (2010) 306–315.

[9] Z. Kulcsár, L. Augsburger, P. Reymond, V. M. Pereira, S. Hirsch, A. S. Mallik, J. Millar, S. G. Wetzel, I. Wanke, D. A. Rüfenacht, Flow diversion treatment: Intra-aneurismal blood flow velocity and WSS reduction are parameters to predict aneurysm thrombosis, Acta Neurochirurgica 154 (10) (2012) 1827–1834.

[10] I. Larrabide, M. L. Aguilar, H. G. Morales, A. J. Geers, Z. Kulcsár, D. A. Rüfenacht, a. F. Frangi, Intra-aneurysmal pressure and flow changes induced by flow diverters: Relation to aneurysm size and shape, American Journal of Neuroradiology 34 (4) (2013) 816–822.

[11] Y. Zhang, W. Chong, Y. Qian, Investigation of intracranial aneurysm hemodynamics following flow diverter stent treatment, Medical Engineering & Physics 35 (5) (2013) 608–615.

[12] F. Mut, J. R. Cebral, Effects of flow-diverting device oversizing on hemodynamics alteration in cerebral aneurysms, American Journal of Neuroradiology 33 (10) (2012) 2010–2016.

[13] M. R. Levitt, P. M. McGah, A. Aliseda, P. D. Mourad, J. D. Nerva, S. S. Vaidya, R. P. Morton, B. V. Ghodke, L. J. Kim, Cerebral aneurysms treated with flow-diverting stents: Computational models with intravascular blood flow measurements, American Journal of Neuroradiology 35 (1) (2014) 143–148.

[14] F. Mut, D. Ruijters, D. Babic, C. Bleise, P. Lylyk, J. R. Cebral, Effects of changing physiologic conditions on the in vivo quantification of hemody-

namic variables in cerebral aneurysms treated with flow diverting devices, International Journal for Numerical Methods in Biomedical Engineering 30 (1) (2014) 135–142.

[15] M. Cavazzuti, M. A. Atherton, M. W. Collins, G. S. Barozzi, Non-Newtonian and flow pulsatility effects in simulation models of a stented intracranial aneurysm, Proceedings of the Institution of Mechanical Engineers, Part H: Journal of Engineering in Medicine 225 (6) (2011) 597–609.

[16] C. Sadasivan, L. Cesar, J. Seong, A. Rakian, Q. Hao, F. O. Tio, A. K. Wakhloo, B. B. Lieber, An original flow diversion device for the treatment of intracranial aneurysms: Evaluation in the rabbit elastase-induced model, Stroke 40 (3) (2009) 952–958.

[17] V. M. Pereira, O. Bonnefous, R. Ouared, O. Brina, J. Stawiaski, H. Aerts, D. Ruijters, A. P. Narata, P. Bijlenga, K. Schaller, K. O. Lovblad, A DSA-based method using contrast-motion estimation for the assessment of the intra-aneurysmal flow changes induced by flow-diverter stents, American Journal of Neuroradiology 34 (4) (2013) 808–815.

[18] M. C. Villa-Uriol, G. Berti, D. R. Hose, A. Marzo, A. Chiarini, J. Penrose, J. Pozo, J. G. Schmidt, P. Singh, R. Lycett, I. Larrabide, A. F. Frangi, @neurIST complex information processing toolchain for the integrated management of cerebral aneurysms, Interface Focus 1 (3) (2011) 308–319.

[19] A. Chien, M. A. Castro, S. Tateshima, J. Sayre, J. R. Cebral, F. Viñuela, Quantitative hemodynamic analysis of brain aneurysms at different locations, American Journal of Neuroradiology 30 (8) (2009) 1507–1512.

[20] H. Bogunović, J. M. Pozo, M. C. Villa-Uriol, C. B. Majoie, R. van den Berg, H. A. F. G. van Andel, J. M. Macho, J. Blasco, L. S. Román, A. F. Frangi, Automated segmentation of cerebral vasculature with aneurysms in 3DRA and TOF-MRA using geodesic active regions: An evaluation study, Medical Physics 38 (1) (2011) 210–222.

[21] I. Larrabide, M. C. Villa-Uriol, R. Cárdenes, V. Barbarito, L. Carotenuto, A. J. Geers, H. G. Morales, J. M. Pozo, M. D. Mazzeo, H. Bogunović, P. Omedas, C. Riccobene, J. M. Macho, A. F. Frangi, AngioLab – A software tool for morphological analysis and endovascular treatment planning of intracranial aneurysms, Computer Methods and Programs in Biomedicine 108 (2) (2012) 806–819.

[22] I. Larrabide, M. Kim, L. Augsburger, M. C. Villa-Uriol, D. A. Rüfenacht, A. F. Frangi, Fast virtual deployment of self-expandable stents: Method and in vitro evaluation for intracranial aneurysmal stenting, Medical Image Analysis 16 (3) (2012) 721–730.

[23] S. Appanaboyina, F. Mut, R. Löhner, C. M. Putman, J. R. Cebral, Simulation of intracranial aneurysm stenting: Techniques and challenges, Computer Methods in Applied Mechanics and Engineering 198 (45).

[24] H. G. Morales, I. Larrabide, A. J. Geers, M. L. Aguilar, A. F. Frangi, Newtonian and non-Newtonian blood flow in coiled cerebral aneurysms, Journal of Biomechanics 46 (13) (2013) 2158–2164.

[25] A. Bernardini, I. Larrabide, H. G. Morales, G. Pennati, L. Petrini, S. Cito, A. F. Frangi, Influence of different computational approaches for stent deployment on cerebral aneurysm haemodynamics, Interface Focus 1 (3) (2011) 338–348.

[26] M. Tremmel, J. Xiang, Y. Hoi, J. Kolega, A. H. Siddiqui, J. Mocco, H. Meng, Mapping vascular response to in vivo hemodynamics: Application to increased flow at the basilar terminus, Biomechanics and Modeling in Mechanobiology 9 (4) (2010) 421–434.

[27] M. P. Szymanski, E. Metaxa, H. Meng, J. Kolega, Endothelial cell layer subjected to impinging flow mimicking the apex of an arterial bifurcation, Annals of Biomedical Engineering 36 (10) (2008) 1681–1689.

[28] Y. Nakayama, Introduction to Fluid Mechanics, Butterworth-Heinemann, 1999.

[29] M. Kim, D. B. Taulbee, M. Tremmel, H. Meng, Comparison of two stents in modifying cerebral aneurysm hemodynamics, Annals of Biomedical Engineering 36 (5) (2008) 726–741.

[30] S. Cito, M. D. Mazzeo, L. Badimon, A review of macroscopic thrombus modeling methods, Thrombosis Research 131 (2) (2013) 116–124.

[31] J. J. Schneiders, E. VanBavel, C. B. Majoie, S. P. Ferns, R. van den Berg, A flow-diverting stent is not a pressure-diverting stent, American Journal of Neuroradiology 34 (1) (2013) E1–4.